Steplike Switching in Symmetric $PbZr_{0.2}Ti_{0.8}O_3/CoFeO_4/PbZr_{0.2}Ti_{0.8}O_3$ Heterostructures for Multistate Ferroelectric Memory

Andra Georgia Boni, Cristina Chirila, Iuliana Pasuk, Raluca Negrea, Ioana Pintilie, and Lucian Pintilie[*]

National Institute of Materials Physics, Atomistilor 405A, Magurele 077125, Romania

A hysteresis loop with three polarization states is obtained in the case of a symmetric epitaxial ferroelectric-interlayer-ferroelectric structure with bottom and top $SrRuO_3$ electrodes. The ferroelectric layers are of $PbZr_{0.2}Ti_{0.8}O_3$, while the interlayer is $CoFe_2O_4$. It is shown that the three polarization states can be separately accessed, suggesting that this type of structure can be used as building element for a three-state nonvolatile ferroelectric random-access memory (FERAM). The presence of the three-state memory effect is explained through a simple phenomenological model based on Landau-Ginzburg-Devonshire theory. The findings of this study can pave the way to multistate all-oxide FERAM devices, resulting in a 50% increase in the storage density compared to actual nonvolatile memories.

I. INTRODUCTION

The accelerated growth of the number of devices and digital services used for an extremely wide range of situations has generated an enormous production of data. In order to use and process them, these data must be stored in memory devices. One of the main objectives of nonvolatile memory hardware is, thus, to increase the storage capacity by keeping the production costs as low as possible. There are several types of nonvolatile memory, such as flush memory, ferroelectric random-access memory (FERAM), magnetic random-access memory (MRAM), phase-change memory, and resistive random-access memory (RRAM) [1]. In all cases, the memory function derives from a system having two stable states that can be interchanged by applying a suitable external stimulus (e.g., voltage for FERAM or RRAM, or magnetic field for MRAM). The result is that memories that have multiple stable states per element represent a promising alternative to increase the storage density keeping the same number of elements.

For the development of future technologies, there is increased interest in multiferroic materials, which by definition have at least two ferroic ordering parameters, each with two possible states [2–4]. This property makes possible the existence of multibit memory devices [5–7]. In particular, these memory cells have different potential states assigned to stable magnetic and/or ferroelectric ordering, and the existence of extra ones can be obtained if coupling between them is possible. In addition to the studies addressing the coexistence and the coupling of different ferroic order parameters in ferromagnetic or ferroelectric multilayers and multiferroic tunnel junctions, another interesting and less exploited topic possibly leading

to multistate memory cells is the presence of multiple (steplike) ferroelectric switching. Getting more than two stable ferroelectric polarization states provides another opportunity to increase the density of stored information in memory cells.

The study of multilayered ferroelectric thin films has shown that the effects produced by the interfacial coupling and the different thicknesses of the component layers are not trivial. One of the possible properties, thus, obtained is the ferroelectric or antiferroelectric coupling of the polarization in some superlattices. This topic has been exploited, especially in terms of theory in numerous scientific papers [8–15], which shows that different parameters, such as the strength of the coupling or the thickness of the interfacial layer, can change the shape of the hysteresis curve from typical ferroelectric to antiferroelectric, highlighting the ability to obtain multistate ferroelectric memories. Many of these studies are speculative by not providing information about how they can get such coupling in practice [8,9].

From the experimental point of view, multiple (steplike) switching hysteresis loops of ferroelectric polarization have been reported only in the last five to six years in various types of structures (to the best of our knowledge) [16–22]. The reported results are explained based on different effects or geometries of the studied structures. For example, the use of modulation or variation in the thickness of the ferroelectric layer in a capacitor cell type [16] or building a structure consisting of two vertically stacked capacitors with different thicknesses of the ferroelectric layer [21]. Another example is the artificial generation of multiple switching controlled by inducing a field generated by the permanent dipoles associated to structural defects (defect engineering). A further example is the different configurations of the heterostructures such as the ferroelectric field-effect transistor [17] or ferroelectric-insulator-semiconductor stacks [18], for which three stable states of

[*]Corresponding author.
pintilie@infim.ro

polarization are obtained. Finally, multiple current peaks were observed in $PbTiO_3/CaTiO_3$ superlattices, but the possible memory effect was not investigated [22].

In this study, we experimentally prove the presence of three different ferroelectric polarization states in a symmetric multilayered $PbZr_{0.2}Ti_{0.8}O_3/CoFe_2O_4/PbZr_{0.2}Ti_{0.8}O_3$ (PZT/CFO/PZT) structure. We first show that this property is dependent on different conditions such as the temperature and strain or structural quality of the ferroelectric layers, and we speculate that this ferroelectric behavior can have as possible sources the different properties of the two PZT layers (one more strained and deposited on the bottom metallic $SrRuO_3$ electrode and the other more relaxed and deposited on the higher-resistivity CFO layer) and a flexoelectric field induced by the strain gradient between the PZT layers. In the last part, we use a thermodynamic phenomenological model in which by considering the depolarization field contribution (induced at the interfaces between the PZT layers and the CFO interlayer), we show that the existence of a third minimum in free energy is possible. Two of the minima are attributed to normal polarization states, while the third minimum is associated to a state with zero total polarization due to either head-to-head or tail-to-tail polarization alignment in the two ferroelectric layers.

II. EXPERIMENT

A. Growth of the structures

The structures are grown by pulsed laser deposition (PLD) on single-crystal $SrTiO_3$ (STO) substrates with (001) orientation. The PLD workstation (Surface-Tec GmbH) is equipped with an excimer laser (KrF, 248-nm wavelength, 700-mJ energy, up to 10-Hz repetition rate), a heated substrate holder, a four-target carrousel, and an automatic control of the laser fluence. Ceramic targets of the desired composition are used for deposition.

First, a bottom $SrRuO_3$ (SRO) or $La_{0.7}Sr_{0.3}MnO_3$ (LSMO) electrode of about 20 nm thickness is deposited. The deposition conditions for the bottom electrode are as follows: substrate temperature of $T = 700\,°C$, background atmosphere of 13.3-Pa oxygen, and laser fluence of 2 J/cm^2 for the SRO; substrate temperature of $T = 600\,°C$, background atmosphere of 15-Pa oxygen, and laser fluence of 0.4 J/cm^2 for the LSMO. The deposition conditions for the PZT layers are substrate temperature of $T = 575\,°C$, background atmosphere of 20-Pa oxygen, and laser fluence of 2 J/cm^2, while for the CFO layer, the conditions are substrate temperature of $T = 600\,°C$, background atmosphere of 20-Pa oxygen, and laser fluence of 1.5 J/cm^2.

B. Characterization methods

The structural quality of the samples is checked by x-ray diffraction (XRD) using Cu $K\alpha$ radiation (Bruker D8 Advance). TEM investigations are performed on a probe-corrected JEM-ARM200F electron microscope. The cross-section specimens for the TEM observations are prepared by mechanical polishing followed by ion milling at low angle in a Gatan PIPS installation. The top SRO contacts for electrical measurements are deposited using a shadow mask. All the hysteresis measurements, including those specific for ferroelectric memories (retention), are performed using a ferritester (model TF 2000 from aixACCT). The temperature-dependent measurements are performed by inserting the samples into a micromanipulated cryostation (Lake Shore model CPX-VF).

III. RESULTS AND DISCUSSION

A. Structure

The XRD patterns of the samples are presented comparatively in Fig. 1. The CFO, with face-centered symmetry, has only two lines, 004 and 008, on the measured 2θ range (15°–120°), unlike the other structures, which have primitive cells, thus, showing all four maxima (001, 002, 003, and 004). These two CFO peaks are clearly evidenced in the XRD pattern of PZT/CFO/PZT/LSMO. The lattice constant of the CFO perpendicular to the substrate is $c = 8.380$ Å, as in bulk CFO with cubic symmetry (according to the ICDD card no. 22-1086). On the XRD pattern of PZT/CFO/PZT/SRO, one can observe the splitting of all four PZT lines. The two peaks giving two different out-of-plane lattice parameters can be associated with the two PZT layers at the bottom and top of the CFO. A shallow third peak is also evidenced, corresponding to a smaller out-of-plane lattice parameter, suggesting an almost fully relaxed PZT layer. The association of this peak with a more relaxed PZT structure is supported by its very similar position with that of PZT in a PZT/CFO/PZT/LSMO heterostructure. The structural information is completed by reciprocal-space mappings around the node of the (-103) STO tilted plane, wherefrom one can obtain also the in-plane parameters of the films (Fig. 2). The low-intensity 206 node of CFO, which should lie in this region, is not detected, so that the in-plane parameter of CFO is not determined. Both SRO and LSMO look to be fully strained (with the in-plane parameters fully adapted to the STO substrate). The shape of the intensity map around PZT on PZT/CFO/PZT/SRO evidences the three nodes. The node noted as PZT1 shows an in-plane parameter very close to that of the SRO underlayer, indicating an almost fully strained PZT ($a = 3.905$ Å, $c = 4.225$ Å), probably originated from the bottom PZT film. The node PZT2 belongs to a partially relaxed epitaxial PZT structure ($a = 3.936$ Å, $c = 4.170$ Å). The PZT3 node is in a position similar to that of the PZT node in PZT/CFO/PZT/LSMO, giving the following lattice parameters: $a = 3.957$ Å, $c = 4.110$ Å, which indicate a tensile in-plane strain (compared to a bulk tetragonal $PbZr_{0.2}Ti_{0.8}O_3$, $a = 3.9539$ Å, $c = 4.1319$ Å, ICDD file no. 70-4260). This fact suggests that this PZT
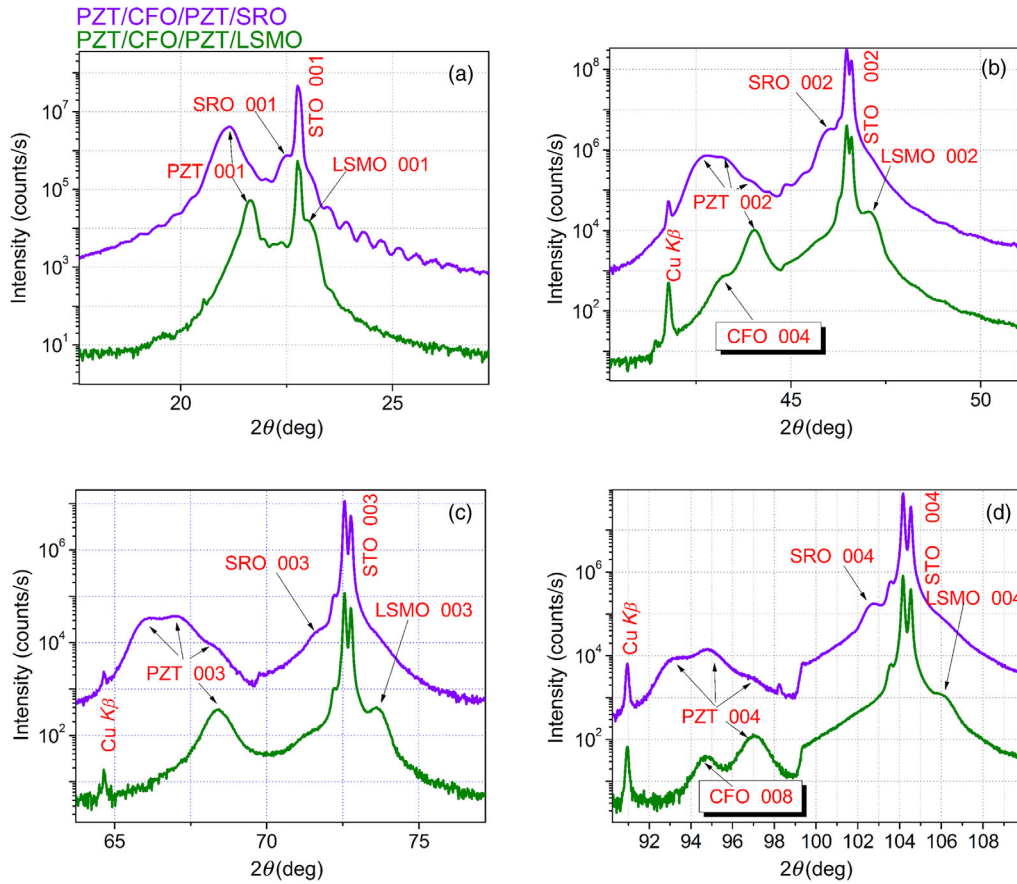
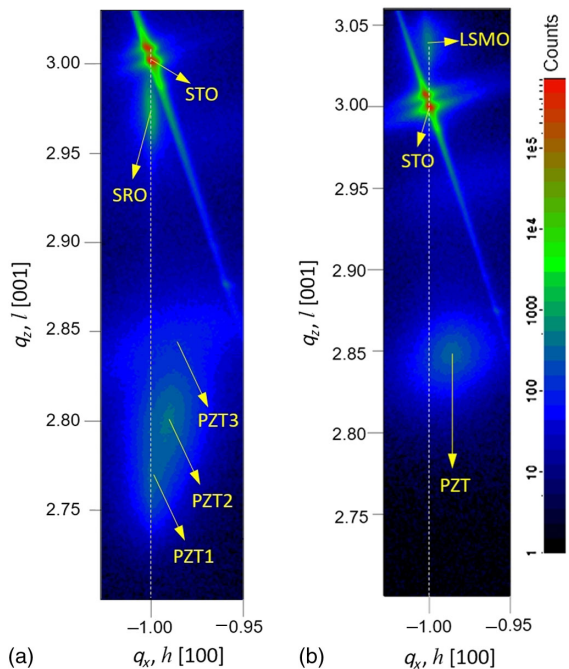FIG. 1. The XRD patterns (2θ-ω scans) enlarged near STO 001 (a), 002 (b), 003 (c), and 004 (d) maxima.

FIG. 2. Reciprocal-space mappings around STO-103. (a) PZT/CFO/PZT/SRO, (b) PZT/CFO/PZT/LSMO.

layer grown over CFO is trying to adapt the in-plane parameter to the larger one of CFO. It is worth noting that the intensities of the PZT3 peaks (and node) are much lower (with approximately 1 order of magnitude) than those of PZT1 and PZT2, indicating the small weight of this phase in the structure with the films grown on the SRO bottom electrode.

Conventional TEM images [Figs. 3(a) and 3(c)] show the distribution and the morphology of the thin layers in the PZT/CFO/PZT/LSMO/STO and PZT/CFO/PZT/ SRO/STO heterostructures. The thickness of PZT is about 50 nm and CFO about 30 nm for both heterostructures, the LSMO layer is 30 nm, and SRO is about 20 nm. The selected area electron diffraction (SAED) patterns [Figs. 1(b) and 1(d)] from the entire structure prove the epitaxial growth of the LSMO/SRO, PZT, and CFO layers on the STO (001) substrate. In both cases, the micrographs are recorded along the $[100]_{STO}$ zone axis of the cubic perovskite substrate. The SAED patterns indicate that the PZT layers have tetragonal phase even if they are grown on LSMO or SRO. The epitaxial LSMO layer has a tetragonal phase with the space group $I4/mcm$ and the SRO ortho-rhombic phase with the space group $Pbnm$. The CFO layer between the PZT layers has cubic structure with $a = b = c = 8.39$ Å and space group $Fd3m$. The doubled (001) spots in the diffraction patterns reveal the misfit between the PZT thin film and the STO (001) substrate.
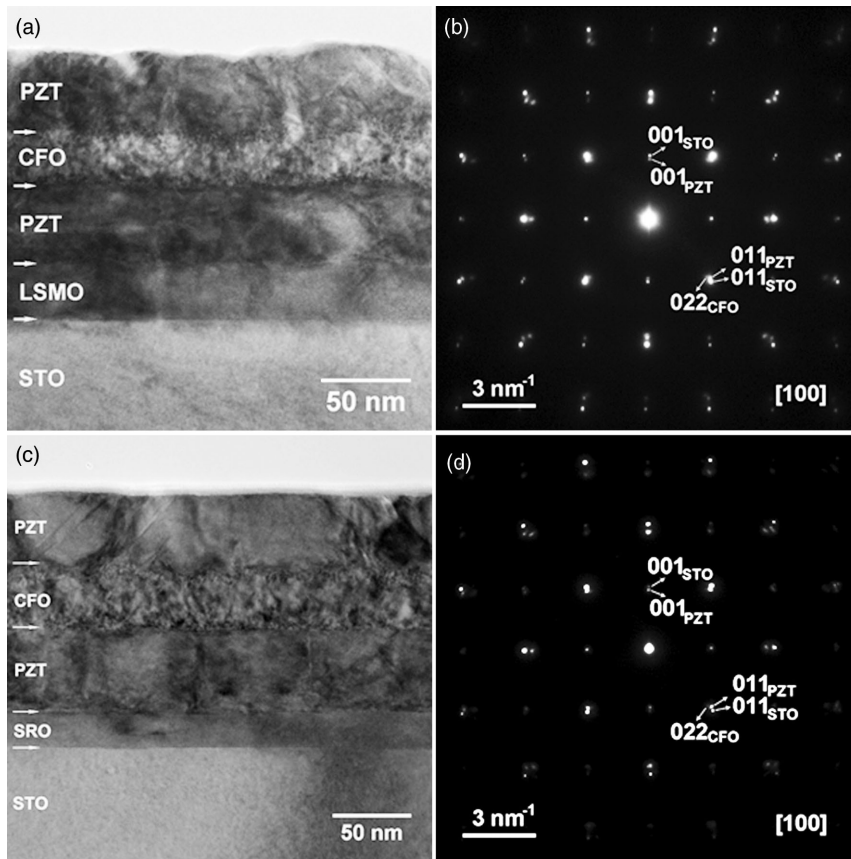
FIG. 3. (a),(c) TEM images at low magnification showing PZT/CFO/PZT/LSMO/STO and PZT/CFO/PZT/SRO/STO heterostructures; (b),(d) SAED patterns corresponding to TEM images (a) and (c), respectively.

The orientation relationship between the crystallographic axis of the CFO and PZT layers with respect to the STO substrate in the case of both heterostructures is $[011]_{STO} \| [011]_{PZT} \| [022]_{CFO}$. The mismatch between the LSMO or SRO and STO substrate is about 1%, resulting in an overlap of the diffraction spots in the SAED patterns.

From conventional TEM (CTEM), images can be observed in which the surface and interfaces are smooth in the PZT/CFO/PZT/SRO/STO heterostructure, and the PZT thin films grow uniform, while in the PZT/CFO/PZT/LSMO/STO heterostructure, the interfaces and surface have higher roughness. The CFO layer has the same pyramidal growth in both cases. The dark contrast from the CTEM images in the vicinity of the interfaces indicates the presence of the mismatch strain field, and the dark contrast inside the layers indicates the strain field due to the

structural defects. Further details on the structural characterization can be found in Refs. [4,23].

B. Ferroelectric properties

The ferroelectric behavior is usually studied by performing dynamic hysteresis measurements in the dynamic mode. A triangular voltage wave of a given amplitude and frequency is applied on the sample for this purpose. The current and charge are recorded, while the variable voltage is applied, giving the current or/and charge (polarization) hysteresis loops. The current loops obtained in this way for the structure deposited on the SRO bottom electrode are presented in Fig. 4 for low amplitude of the applied voltage (named unsaturated hysteresis) and for higher amplitude of the applied voltage (named saturated
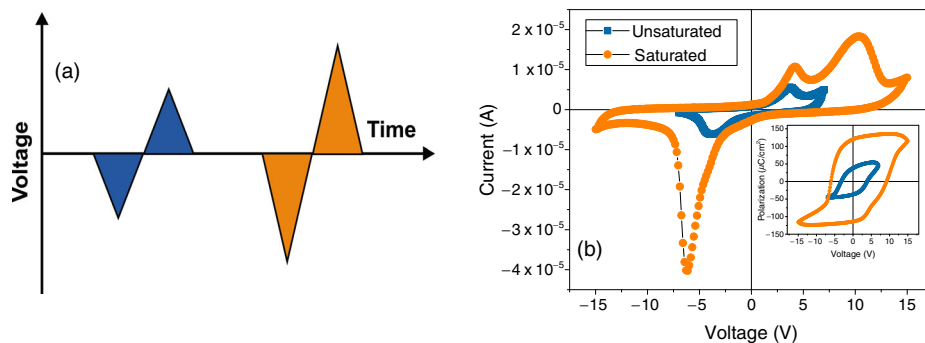

FIG. 4. (a) The train of voltage pulses used for hysteresis measurements; (b) the current hysteresis at low voltage (unsaturated) and high voltage (saturated). The inset shows the polarization hysteresis. The measurement as performed at the frequency of 100 Hz of the applied triangular wave on PZT/CFO/PZT/SRO/STO.
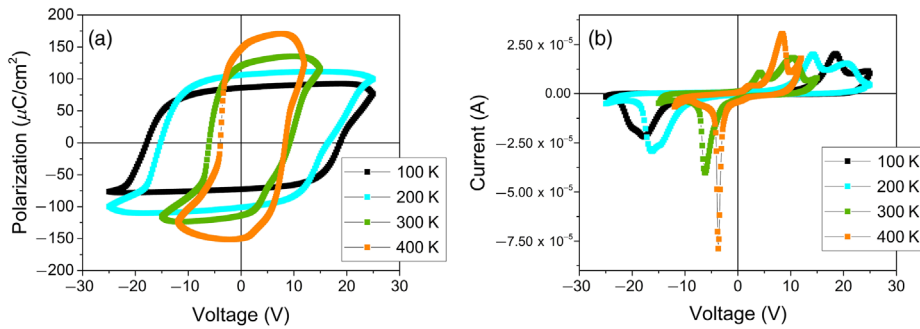
FIG. 5. (a) The polarization hysteresis and (b) the current hysteresis recorded at different temperatures for a PZT/CFO/PZT/SRO/STO structure at 100 Hz.

hysteresis). Both unsaturated and saturated loops present peaks which are associated to the polarization reversal. One can see that two distinct switching peaks are present for positive polarity when external voltage with higher amplitude is applied on the sample to obtain polarization saturation. This result suggests that the polarization switching takes place in two steps with different values of the coercive field.

The ferroelectric behavior is further studied by performing dynamic hysteresis measurements for different temperatures. The evolution of the saturated polarization loop with increasing the temperature is presented in Fig. 5 for the heterostructure deposited on the bottom SRO electrode. One can observe that steplike switching appears to be present for all temperatures and that the value of the remnant polarization is about 90 μC/cm^2 in all cases after making the correction for the leakage current contribution. This value is in good agreement with previously reported values for PbZr$_{0.2}$Ti$_{0.8}$O$_3$ epitaxial thin films [24,25]. Other observations regarding Fig. 5 are as follows:

(a) The coercive field decreases significantly with increasing temperature, from about 1400 kV/cm at 100 K to about 470 kV/cm at 400 K. The values are slightly larger than for a single PZT layer (usually in the 100–400 kV/cm range at room temperature, depending on thickness and structural quality [26–28]), probably due to the presence of the CFO interlayer.

(b) An internal electric field exists in the structure oriented towards the top contact. The magnitude of this field averaged on the entire thickness of the structure increases with increasing temperature, from about 38 kV/cm at 100 K to about 170 kV/cm at 400 K. Such internal fields exist also in single PZT layers grown on the SRO bottom electrodes [29]. There are several causes that can lead to the occurrence of an internal electric field, such as a strain gradient [26], a nonuniform distribution of charged defects, or nonsymmetric potential barriers at the electrode interfaces [30]. According to the structural investigations, it may be that the differences between the two PZT layers may contribute to the occurrence of the internal field in the case of the studied PZT/CFO/PZT/SRO/STO structure.

(c) Regarding the steplike switching, it seems that this is more clearly visible at lower temperatures (below

300 K). Also, the steplike switching is clearer on the positive polarity of the voltage applied on the top electrode. Two distinct current peaks occur in this case (see Fig. 4 also) at 200 and 300 K. For negative voltage, there are no distinct peaks, although at 100 and 200 K, the current peak seems to be the result of merging two peaks (see the evident asymmetry of the peak at this temperatures). The peak on the negative voltage becomes narrower and relatively symmetric with increasing temperature, while the peaks on the positive polarity merge as one as the temperature increases to 400 K.

(d) The switching kinetics seems to be different for negative and positive polarity. Considering only the results at 400 K, one can see that the current peak is sharp and with high value of current when the polarization switches from downward (from top to bottom electrode) to upward direction and is wide and with lower value of current when the polarization switches from upward to downward orientation. Such a behavior may be attributed to the presence of the internal electric field favoring the upward polarization, thus, making the switching faster when polarization changes from the downward to upward direction.

The temperature dependence of the hysteresis loop for the case of the PZT/CFO/PZT heterostructure deposited on the bottom LSMO contact is presented in Fig. 6. The value of the remnant polarization is around 70 μC/cm^2 after subtracting the contribution of the leakage current, which is lower than for the heterostructure deposited on the SRO electrode.

From Fig. 6, one can also observe the following:

(a) The coercive field varies from about 1340 kV/cm at 100 K to about 550 kV/cm at 300 K. At 400 K, the structure seems to degrade due to a large increase in the leakage current, especially on negative polarity.

(b) The steplike switching is present, especially at low temperature [see the current hysteresis at 100 K in Fig. 6(b)] but is less visible compared to the PZT/CFO/PZT structure on the SRO electrode. One can notice that at 300 K, the steplike switching is no longer visible in the current hysteresis.

(c) The hysteresis loops appear to be almost symmetric compared to the structure deposited on SRO.
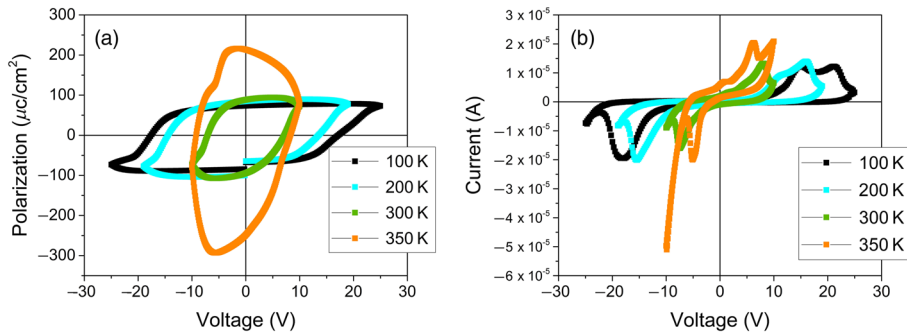
FIG. 6. (a) The polarization hysteresis and (b) the current hysteresis recorded at different temperatures for a PZT/CFO/PZT/LSMO/STO structure at 100 Hz.

However, an internal electric field also exists in the case of the structure deposited on LSMO, but its value is significantly lower (just 7.7 kV/cm at room temperature compared to 120 kV/cm for the structure on SRO), and its direction is towards the bottom LSMO electrode (internal field oriented towards the top contact for the structure on SRO).

The differences observed in the hysteretic behavior of the PZT/CFO/PZT heterostructures deposited on different bottom electrodes (SRO and LSMO) correlate well with the results of the structural characterization. In the case of the structure deposited on the bottom LSMO electrode, it appears that both PZT layers are relaxed, with low values for the lattice constant on the *c* direction, leading to small tetragonality and low values for the remnant polarization and coercive field [27,29]. On the other hand, in the case of the structure deposited on the SRO bottom electrode, three distinct values are obtained from XRD patterns for the *c* lattice constant of PZT. These may be interpreted in the following way: The highest value for the *c* constant corresponds to the PZT layer deposited directly on SRO due to the compressive stress imposed by the substrate; the intermediate *c* value may correspond to the PZT film deposited on the CFO film; the lowest *c* value may correspond to a very thin PZT layer just above the CFO film, a layer with higher density of structural defects as revealed by TEM analysis (see Fig. 3). It seems that the differences in the structural quality of the PZT layers inside the PZT/CFO/PZT heterostructures lead to the differences observed in the hysteretic behavior, such as follows:

(a) Higher polarization value, 90 μC/cm^2, for the structure grown on SRO compared to 70 μC/cm^2 for the structure deposited on the LSMO bottom electrode.

(b) Different values for the internal electric field, which are higher in the strained structure grown on SRO and almost absent for the structure grown on LSMO.

(c) Different switching behaviors, referring to the steplike switching. The phenomenon is clearly visible for positive voltages in the case of the structure deposited on the SRO electrode [see Fig. 5(b)], but it is less visible for the structure deposited on the LSMO contact, where the steplike switching seems to be present only at low temperatures [see Fig. 6(b)]. For both structures, the phenomenon is hardly visible on negative voltages, except maybe for low temperatures in the case of the structure deposited on SRO when a shoulder in the current peak associated to polarization switching can be observed [see Fig. 5(b)].

The above presented results show that the introduction of the CFO interlayer is disrupting the structural properties of the PZT layers inducing a strain gradient. This, in turn, appears to produce an internal electric field which influences the polarization switching, leading to steplike switching in the PZT/CFO/PZT structure. This behavior is more visible for the structure grown on SRO, in relation with the better quality of the structure in this case compared to the one grown on the LSMO bottom contact. The main consequence is that the polarization switching is altered, and hysteresis loops with three or more different polarization states can be obtained, as revealed by the presence of at least three distinct switching peaks in the current hysteresis loop presented in Figs. 5(b) and 6(b).

Having three possible polarization states, one can hypothesize that the studied PZT/CFO/PZT structures can be possible solutions for a 50% increase in the memory density of the ferroelectric RAM memory cells. Figure 7(a) shows a schematic representation of the pulse sequence used to experimentally access all three polarization states by writing or reading processes. The polarization states named $P0$ and $P2$ are written by applying a 14-V triangle pulse with negative and positive polarity, respectively. The $P1$ polarization state is written by applying a 14-V negative pulse followed by a 7-V positive pulse. The writing of this different polarization state is marked by switching peaks in current measurements during these pulses. The read operation is done by recording the current during a 14-V positive voltage pulse [Fig. 7(b)]. The charge recorded on the read pulse is obtained by $Q_{\mathrm{sw}} = (1/A)(dt/dV)\int_0^V I\,dV$, and it is represented in Fig. 7(c) for the three written polarization states. Obtaining different electrical responses (as current or integrated charge) on this read pulse proves that there are indeed three different polarization states.

The retention is an important property of a FERAM memory defined as the ability to store a certain polarization state as much as possible and is a qualitative description of the nonvolatility. The standard retention measurement is the schematic represented in Fig. 8(a): A triangular writing
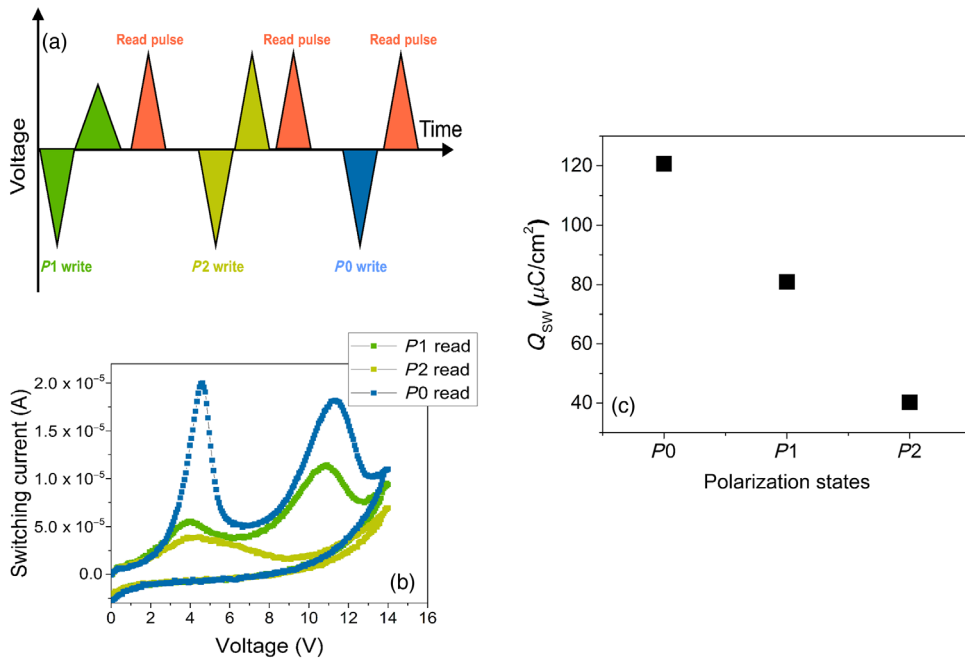
FIG. 7. (a) The voltage train pulse used to write and read different memory states in the PZT/CFO/PZT structure grown on a bottom SRO electrode; (b) the recorded currents for the read pulse; (c) the charge calculated with the formula mentioned in the main text.

pulse is applied to the capacitor structure with amplitude 7, 14, or −14 V, respectively, to set one of the three polarization states. A read pulse with the same amplitude as the writing pulse is applied after a certain period of time (retention time). During the read pulse, a current is recorded which has, in addition to the usual contribution from dielectric displacement and leakage current, also a back-switching contribution that occurs during the retention waiting time [see Fig. 8(a)]. The retained value of the polarizations is obtained by subtraction of the read charge
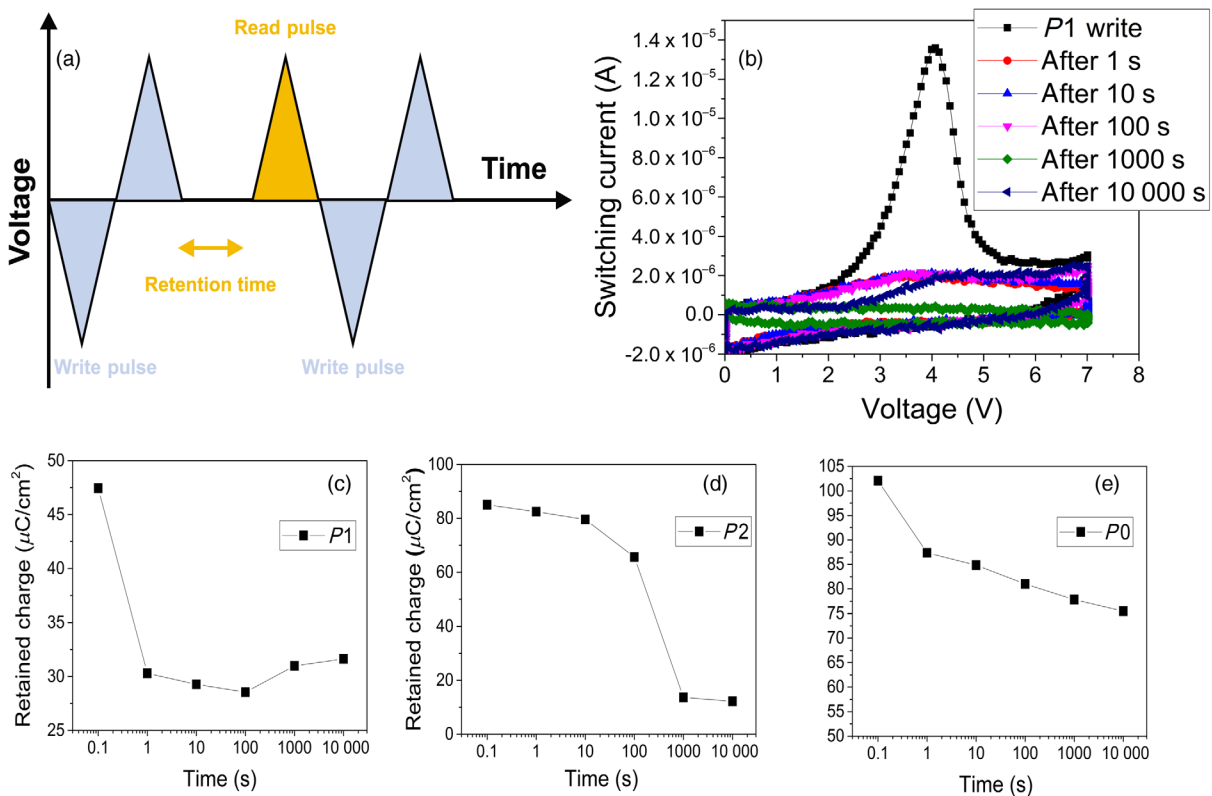

FIG. 8.　(a) The voltage pulse sequence used for retention measurements; (b) the current recorded during the read pulse; (c), (d), and (e) are the retention behavior for the $P1$, $P2$, and $P0$ states, respectively.

from the written charge ($Q_{\text{retained}} = Q_{\text{written}} - Q_{\text{read}}$). This sequence is repeated with different retention time (up to 10^5 s) for all polarization states, and the results are presented in Figs. 8(c)–8(e).

For the $P1$ polarization state, the written pulse set the polarization value to 47 μC/cm^2. After 1 s, the polarization decreases to 30 μC/cm^2 due to backswitching dipoles marked by a small peak in current for the read pulse. This polarization state is the most stable in time, the values of 30 μC/cm^2 being maintained for all 10^5 s. For the case of the $P2$ state, there is a very small variation in the first 10 s, but then an abrupt decreasing of the retained charge towards 10 μC/cm^2 occurs. A decrease of the retained charge can be observed for the $P0$ state, in the first second, similar to the $P1$ state, followed by only a 10% variation after 10^5 s. The different depolarization tendencies for the three polarization states are caused by different compensation mechanisms of the polarization charges and the presence of the internal electric field, as we discuss in the next subsection.

C. Discussion

As we show above, our main experimental result consists of obtaining at least three distinct states of the ferroelectric polarization in a multilayered PZT/CFO/PZT structure. The distinct states are associated to the successive current peaks observed in the current hysteresis loop and correspond to a steplike switching of the polarization as shown in Figs. 5 and 6. The "separation" between the polarization states in term of voltages where the current peaks occur is dependent on structural quality and temperature. The present result points out that the steplike switching with three states is more visible for the structures deposited on SRO, probably due to the different strain conditions in the two PZT layers, as revealed by the XRD investigations. One has to point out that the present case is different from previous reports. For example, the design of the structure is different (symmetric ferroelectric-interlayer-ferroelectric) compared to the report showing three ferroelectric states in an asymmetric metal-ferroelectric-insulator-semiconductor-metal structure [19]. Also, the mechanism leading to the occurrence of more than two polarization states is different compared to previous reports [18,20].

A very simple explanation for the observed phenomenon is to assume that the polarization switching takes place successively in the two ferroelectric layers. Two current peaks can be obtained in this case, both having the same sign. These aspects are discussed in more detail later. The phenomenon cannot be associated to resistive switching often observed in ferroelectric layers (memristor effect [31]), implying transition from a low resistivity state to a high resistivity state and vice versa. It is not the case in the present study showing that after polarization saturation, the current returns to a lower value. This behavior implies that the current peaks are associated only to polarization
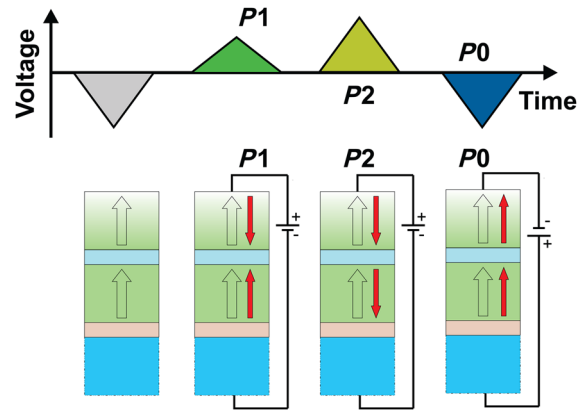

FIG. 9. Schematic of the writing voltage pulses for the three distinct polarization states (upper line) and the corresponding polarization orientations inside the PZT layers of the PZT/CFO/PZT structures.

switching in the two PZT layers. One also has to mention that the hysteresis loops (current and charge) presented in Figs. 4–6 are produced by the entire structure acting as a single capacitor; thus, details on the microscopic behavior of domains and domain walls are less relevant. It may be that local variation in structural quality may affect the domains or domain-wall dynamics, as reported elsewhere [32,33], or the polarization stability in time [23]. In any case, at the macroscale, the result is the one presented in the above-mentioned figures.

To qualitatively explain the multiple switching steps of the ferroelectric polarization, we use the schematic of the structure shown in Fig. 9, in which the orientation of the internal fields (transparent arrow) and polarization (red arrow) as a function of the writing pulses are also presented. The internal fields are considered to point towards the upper surface of the structure, as we find experimentally for the structure deposited on the SRO bottom electrode. As previously mentioned, the internal field can originate from the strain gradient, and its intensity is proportional with the strain gradient [26,34,35]. For the case of the $P2$ and $P0$ states obtained after applying a high-amplitude voltage pulse, one can consider that in both ferroelectric layers, the polarization is oriented either downward ($P2$) or upward ($P0$; see, also, Fig. 9, the upper line). For the intermediate $P1$ state, we can suppose that the polarization inside the structure is in an intermediate state, possible in a head-to-head or tail-to-tail configuration (see Fig. 9, bottom line). As we mention above, a possible scenario is that for positive voltage on the top contact, the switching takes place first in the PZT layer deposited on CFO, leading to the $P1$ state and then in the layer deposited on SRO leading to the $P2$ state. This scenario is in agreement with the values extracted for the lattice constant in the c direction, showing a strained layer on SRO and a more relaxed layer on CFO. One can presume that in the more relaxed layer,

the switching takes place easier and that the internal electric field has a lower magnitude leading to less backswitching and to a relatively stable $P1$ state as shown in Fig. 8(c). Increasing the voltage, the polarization switches also in the PZT layer deposited on SRO, but due to the higher strain, the internal electric field in this layer is larger, thus, leading to significant backswitching that can explain the poor stability of the state $P2$, as shown in Fig. 8(d). One has to mention that the values of the internal field estimated in Sec. III B are obtained as an average over the entire thickness of the structure. It might be that the internal field is much stronger in the PZT films deposited on SRO than in the film deposited on CFO, leading to a poorer retention of the $P2$ state compared to $P1$.

For the negative voltage on the top contact, the polarization is oriented upward, parallel with the internal field. Therefore, this direction is favored, and one can presume that the switching takes place rapidly in the PZT layer deposited on SRO and then in the layer deposited on CFO. The switching is fast enough in both layers to lead to only one current peak for negative polarity. Therefore, no distinct states occur in this case, as shown in the hysteresis loops in Figs. 5 and 6.

Further on, a simple theoretical model is developed to explain the occurrence of multiple polarization states in the PZT/CFO/PZT structure based on Landau-Ginzburg-Devonshire theory. The total free energy F of the system is written as

$$F = l_{F1}F_1(P_1) + l_{F2}F_2(P_2) + l_{CFO}\frac{\varepsilon_0\varepsilon_{CFO}E_{CFO}^2}{2}. \quad (1)$$

Here, l_{F1}, l_{F2}, and l_{CFO} are the relative thickness of the ferroelectric layers and CFO interlayer, $F_1(P_1)$ represent free energy of the first ferroelectric layer with polarization P_1 and $F_2(P_2)$ represent free energy of the second ferroelectric layer with polarization P_2, ε_0 is the dielectric permittivity of vacuum, ε_{CFO} is the dielectric permittivity of CFO, and E_{CFO} is the electric field induced in the CFO layer by the existence of polarization charges at the interfaces between PZT and CFO. Considering the Gauss low at both interfaces between the ferroelectric PZT layers and CFO layer:

$$\varepsilon_0(E_1 + E_{i1}) + P_1 = \sigma_1 + E_{CFO},$$
$$\varepsilon_0(E_2 + E_{i2}) + P_2 = \sigma_2 + E_{CFO}, \quad (2)$$

where E_1, E_2 are electric applied fields on the ferroelectric layers, E_{i1} and E_{i2} are the internal electric field in each ferroelectric layer, P_1 and P_2 are the polarization in each ferroelectric layer, and σ is the charge at the interfaces between the PZT and CFO layers. The origin of the σ charges compensating the bound polarization charges can be different: either charges from the ferroelectric layer having as sources electric active defects (vacancies, other

structural defects) with increased density for the structure deposited on LSMO compared with the one deposited on SRO; either carrier generated in the CFO layer considered as a semiconductor for which there is an increasing of conductivity with the temperature. For negligible density of the compensation charges, there is a significant contribution of E_{CFO} in the total free energy of the system, which can be associated to a depolarization field and can be approximated by $E_{CFO} = [\varepsilon_0(E_{i1} + E_{i2}) + (P_1 + P_2)]/2$ for the open-circuit condition. The total free energy of the system as a function of total polarization $P = P_1 + P_2$ is simulated in Fig. 10(a). When the density of compensation charges is high enough to screen the electric field inside the CFO layer, the above system results in $\varepsilon_0(E_1 + E_{i1}) + P_1 = \varepsilon_0(E_2 + E_{i2}) + P_2$, which is typical for two ferroelectric capacitor series connected, and the free energy of such system is described in Fig. 10(b).
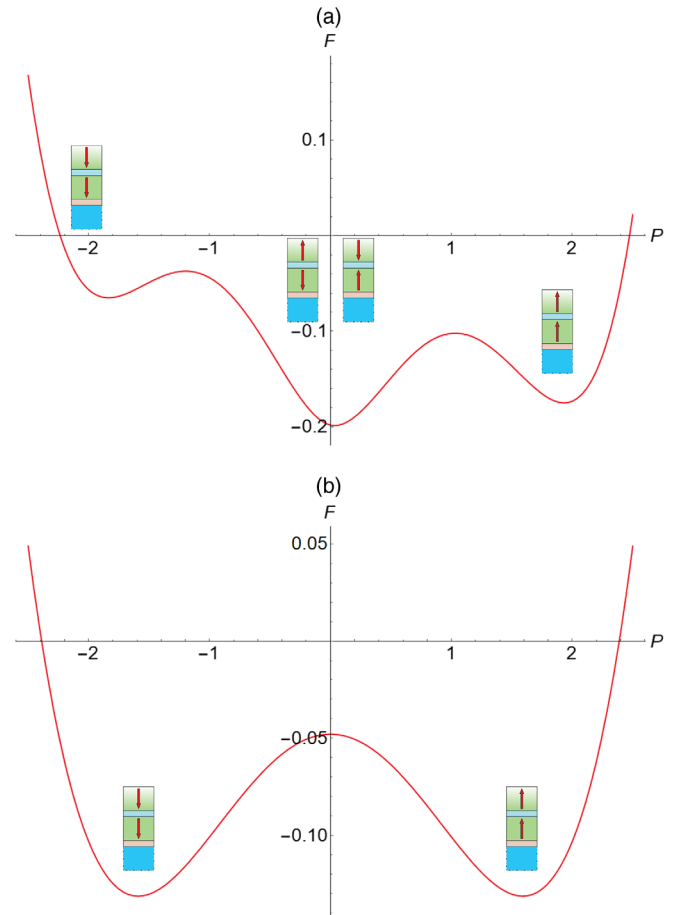

FIG. 10. (a) The free-energy dependence on the total polarization in the case where no free charges are present in the structure; (b) the free-energy dependence on the total polarization in the case where the free charges totally compensate the depolarization fields. The calculations are made for a general PZT-interlayer-PZT structure having the specific case of CFO as an interlayer.

It is obvious that the free energy is totally different for the two cases. When there are sufficient free charges to compensate the polarization charges at all interfaces, the free energy presents only two minima, as for a continuous ferroelectric material, attributed for the two possible orientations of the polarization. When the system lacks the compensation charges, then a depolarization field develops inside the structure, and the dependence of the free energy as a function of total polarization presents three minima instead of two [see Fig. 10(a)]. This result is consistent with the experimental hysteresis loops evidencing three different polarization states in the PZT/CFO/PZT structure. The energy diagram in this case can explain the retention characteristics showing indeed that the less stable state is $P2$ because it is antiparallel with the internal electric field, while $P1$ and $P2$ are stable, although some backswitching also takes place in the states.

One has to mention that the above-described results and model are different from the ones reported in Ref. [22] for $PbTiO_3/CaTiO_3$ superlattices. In the present case is a trilayer structure with thick component films, while in the mentioned reference, it is a multilayer with much thinner component films (only three unit cells for $CaTiO_3$). On the other hand, the multiple current peaks reported in Ref. [22] are associated to gradual polarization rotation as the content of $CaTiO_3$ in the structure increases, resulting in an in-plane polarization for the maximum $CaTiO_3$ content. This is not the case in the present study, as the polarization is assumed to remain out of plane all the time.

Regarding the effect of the CFO thickness on the multistep switching behavior, one can assume that for small thickness the structure may act as a single ferroelectric layer. One can see that the weight of the CFO term to the free energy given by Eq. (1) depends on the thickness of the CFO layer; thus, at very small thicknesses, it is negligible, and the system behaves as a single ferroelectric layer (the two layers are coupled and switch simultaneously, as shown experimentally in Ref. [23] for a trilayer structure with CFO thickness about 15–20 nm). In order to have sequential switching, the two layers have to be decoupled. One can conclude that the CFO layer thickness should be at least 30 nm to have steplike switching.

IV. CONCLUSIONS

PZT/CFO/PZT structures are epitaxially grown by PLD on bottom SRO and LSMO electrodes. The structural analysis reveals significant differences in the structural quality of the PZT films in the two cases and less defective and more strained films when the structure is deposited on the SRO bottom electrode. The investigation of the ferroelectric properties by performing hysteresis measurements reveals the presence of three distinct polarization states: two for positive polarity and one for negative voltages. It is shown that these states are distinct and can be addressed

separately. However, their retention properties are different: two of the states ($P0$ and $P1$) are relatively stable up to 10^4 s, while $P2$ shows a poor retention, the polarization value dropping with about 80% after only 10^3 s. The experimental results are explained by the presence of a significant strain gradient in the structure grown on SRO compared to the one grown on LSMO. The strain difference in the PZT films leads to the occurrence of an internal electric field that favors the upward direction of polarization, leading to a steplike switching of the polarization when positive voltage is applied on the top Pt electrode. A simple thermodynamic model is developed, showing that for certain conditions of the interlayer, three minima can occur in the representation of the free energy as a function of the total polarization in the PZT-interlayer-PZT structure.

The experimental results hint at the possibility to obtain more than three polarization states in such structures by appropriate selection of the interlayer. If the interlayer is CFO, three distinct states can be obtained if the structure is grown on a bottom SRO contact, offering the possibility to increase the storage density by 50% in a FERAM memory cell by replacing the single-layer ferroelectric capacitor with a capacitor based on a PZT/CFO/PZT structure. Further studies are needed to see if more polarization states can be obtained by changing the interlayer and/or by using multiple interlayers. The theoretical model has to be refined also in order to see if more polarization states can be obtained in such structures. Possible refinements should include finite resistance of the ferroelectric and intermediate layers, presence of space-charge regions, and possible coupling between the ferroelectric layers. A more refined model may predict also the optimum thicknesses to obtain clearly distinct and stable polarization states.

ACKNOWLEDGMENTS

[1] L. Wang, C.-H. Yang, and J. Wen, Physical principles and current status of emerging non-volatile solid state memories, Electron. Mater. Lett. **11**, 505 (2015).

[2] M. Bibes and A. Barthélémy, Multiferroics: Towards a magnetoelectric memory, Nat. Mater. **7**, 425 (2008).

[3] W. Eerenstein, N. D. Mathur, and J. F. Scott, Multiferroic and magnetoelectric materials, Nature (London) **442**, 759 (2006).

[4] C. Chirila, G. Ibanescu, L. Hrib, R. Negrea, I. Pasuk, V. Kuncser, I. Pintilie, and L. Pintilie, Structural, electric and magnetic properties of $Pb(Zr_{0.2}Ti_{0.8})O_3$-$CoFe_2O_4$ heterostructures, Thin Solid Films **545**, 2 (2013).

[5] M. Gajek, M. Bibes, S. Fusil, K. Bouzehouane, J. Fontcuberta, A. Barthélémy, and A. Fert, Tunnel junctions with multiferroic barriers, Nat. Mater. **6**, 296 (2007).

[6] D. Bao, Multilayered dielectric/ferroelectric thin films and superlattices, Curr. Opin. Solid State Mater. Sci. **12**, 55 (2008).

[7] K. P. Jayadevan and T. Y. Tseng, Review composite and multilayer ferroelectric thin films: Processing, properties and applications, J. Mater. Sci. Mater. Electron. **13**, 439 (2002).

[8] Y.-Z. Wu, D.-L. Yao, and Z.-Y. Li, Hysteresis loop of a ferroelectric bilayer with an antiferroelectric interfacial coupling, J. Appl. Phys. **91**, 1482 (2002).

[9] K.-H. Chew, L.-H. Ong, J. Osman, and D. R. Tilley, Hysteresis loops of ferroelectric bilayers and superlattices, Appl. Phys. Lett. **77**, 2755 (2000).

[10] L. Cui, T. Lü, X. Xu, and J. Zhou, Theoretical study on the mechanism of abnormal dielectric susceptibility behaviors of ferroelectric bilayer films, J. Appl. Phys. **105**, 104104 (2009).

[11] Z. Chao-Dan, Z. Duan-Ming, L. Xin-Ming, Y. Bin, L. Chao-Jun, and Y. Jun, Effects of depolarization field and interfacial coupling on the polarization of ferroelectric bilayers, Chin. Phys. Lett. **27**, 017702 (2010).

[12] I. Essaoudi, K. Bärner, A. Ainane, and M. Saber, Hysteresis loops of a ferroelectric superlattice with an antiferroelectric interfacial coupling, Phys. Scr. **75**, 500 (2007).

[13] S. Pu-Nan, C. Lian, and L. Tian-Quan, Combined effect of the transition layer and interfacial coupling on the properties of ferroelectric bilayer film, Chin. Phys. B **18**, 1658 (2009).

[14] I. B. Misirlioglu, L. Pintilie, M. Alexe, and D. Hesse, Influence of long-range dipolar interactions on the phase stability and hysteresis shapes of ferroelectric and antiferroelectric multilayers, J. Mater. Sci. **44**, 5354 (2009).

[15] L. Van Lich, T. Shimada, S. Sepideh, J. Wang, and T. Kitamura, Multilevel hysteresis loop engineered with ferroelectric nano-metamaterials, Acta Mater. **125**, 202 (2017).

[16] A. K. Tripathi, A. J. J. M. van Breemen, J. Shen, Q. Gao, M. G. Ivan, K. Reimann, E. R. Meinders, and G. H. Gelinck, Multilevel information storage in ferroelectric polymer memories, Adv. Mater. **23**, 4146 (2011).

[17] B. Kam, X. Li, C. Cristoferi, E. C. P. Smits, A. Mityashin, S. Schols, J. Genoe, G. Gelinck, and P. Heremans, Origin of multiple memory states in organic ferroelectric field-effect transistors, Appl. Phys. Lett. **101**, 033304 (2012).

[18] D. Lee, B. C. Jeon, S. H. Baek, S. M. Yang, Y. J. Shin, T. H. Kim, Y. S. Kim, J.-G. Yoon, C. B. Eom, and T. W. Noh, Active control of ferroelectric switching using defect-dipole engineering, Adv. Mater. **24**, 6490 (2012).

[19] M. H. Park, H. J. Lee, G. H. Kim, Y. J. Kim, J. H. Kim, J. H. Lee, and C. S. Hwang, Tristate memory using ferroelectric-insulator-semiconductor heterojunctions for 50% increased data storage, Adv. Funct. Mater. **21**, 4305 (2011).

[20] W. Hu, Z. Wang, Y. Du, X.-X. Zhang, and T. Wu, Space-charge-mediated anomalous ferroelectric switching in P (VDF-TrEE) polymer films, ACS Appl. Mater. Interfaces **6**, 19057 (2014).

[21] W. Y. Kim and H. C. Lee, Proposal of a ferroelectric multi-bit memory structure for reliable operation at sub-100 nm scale, IET Micro Nano Lett. **10**, 700 (2015).

[22] J. Sinsheimer, S. J. Callori, B. Bein, Y. Benkara, J. Daley, J. Coraor, D. Su, P. W. Stephens, and M. Dawber, Engineering Polarization Rotation in a Ferroelectric Superlattice, Phys. Rev. Lett. **109**, 167601 (2012).

[23] See the Supplemental Material at http://link.aps.org/supplemental/10.1103/PhysRevApplied.8.034035 for high-resolution TEM images and piezoelectric force microscopy investigations at microscale.

[24] I. Vrejoiu, G. Le Rhun, L. Pintilie, D. Hesse, M. Alexe, and U. Gösele, Intrinsic ferroelectric properties of strained tetragonal PbZr$_{0.2}$Ti$_{0.8}$O$_3$ obtained on layer-by-layer grown, defect-free single-crystalline films, Adv. Mater. **18**, 1657 (2006).

[25] I. Pintilie, C. M. Teodorescu, C. Ghica, C. Chirila, A. G. Boni, L. Hrib, I. Pasuk, R. Negrea, N. Apostol, and L. Pintilie, Polarization-control of the potential barrier at the electrode interfaces in epitaxial ferroelectric thin films, ACS Appl. Mater. Interfaces **6**, 2929 (2014).

[26] D. Lee, B. C. Jeon, A. Yoon, Y. J. Shin, M. H. Lee, T. K. Song, S. D. Bu, M. Kim, J.-S. Chung, J.-G. Yoon, and T. W. Noh, Flexoelectric control of defect formation in ferroelectric epitaxial thin films, Adv. Mater. **26**, 5005 (2014).

[27] H. N. Lee, S. M. Nakhmanson, M. F. Chisholm, H. M. Christen, K. M. Rabe, and D. Vanderbilt, Suppressed Dependence of Polarization on Epitaxial Strain in Highly Polar Ferroelectrics, Phys. Rev. Lett. **98**, 217602 (2007).

[28] L. Pintilie, C. Ghica, C. M. Teodorescu, I. Pintilie, C. Chirila, I. Pasuk, L. Trupina, L. Hrib, A. G. Boni, N. Apostol, L. Abramiuc, R. Negrea, M. Stefan, and D. Ghica, Polarization induced self-doping in epitaxial Pb(Zr$_{0.20}$Ti$_{0.80}$)O$_3$ thin films, Sci. Rep. **5**, 14974 (2015).

[29] C. Chirila, A. G. Boni, I. Pasuk, R. Negrea, L. Trupina, G. L. Rhun, S. Yin, B. Vilquin, I. Pintilie, and L. Pintilie, Comparison between the ferroelectric/electric properties of the PbZr$_{0.52}$Ti$_{0.48}$O$_3$ films grown on Si (100) and on STO (100) substrates, J. Mater. Sci. **50**, 3883 (2015).

[30] P. Yua, W. Luob, D. Yia, J. X. Zhanga, M. D. Rosselld, C.-H. Yangf, L. Youg, G. Singh-Bhallaa, S. Y. Yanga, Q. Hea, Q. M. Ramassed, R. Ernid, L. W. Martin, Y. H. Chu, S. T. Pantelides, S. J. Pennycook, and R. Ramesh, Interface control of bulk ferroelectric polarization, Proc. Natl. Acad. Sci. U.S.A. **109**, 9710 (2012).

[31] A. Chanthbouala, V. Garcia, R. O. Cherifi, K. Bouzehouane, S. Fusil, X. Moya, S. Xavier, H. Yamada, C. Deranlot, N. D. Mathur, M. Bibes, A. Barthélémy, and J. Grollier, A ferroelectric memristor, Nat. Mater. **11**, 860 (2012).

[32] G. De Luca, M. D. Rossell, J. Schaab, N. Viart, M. Fiebig, and M. Trassin, Domain wall architecture in tetragonal ferroelectric thin films, Adv. Mater. **29**, 1605145 (2017).

[33] S. Cherifi-Hertel, H. Bulou, R. Hertel, G. Taupier, K. D. Dorkenoo, C. Andreas, J. Guyonnet, I. Gaponenko, K. Gallo, and P. Paruch, Non-Ising and chiral ferroelectric domain walls revealed by nonlinear optical microscopy, Nat. Commun. **8**, 15768 (2017).

[34] B. C. Jeon, D. Lee, M. H. Lee, S. M. Yang, S. C. Chae, T. K. Song, S. D. Bu, J.-S. Chung, J.-G. Yoon, and T. W. Noh, Flexoelectric effect in the reversal of self-polarization and associated changes in the electronic functional properties of BiFeO$_3$ thin films, Adv. Mater. **25**, 5643 (2013).

[35] P. Zubko, G. Catalan, and A. K. Tagantsev, Flexoelectric effect in solids, Annu. Rev. Mater. Res. **43**, 387 (2013).